Graphene-beaded carbon nanofibers for use in supercapacitor electrodes: Synthesis and electrochemical characterization

Zhengping Zhou*, Xiang-Fa Wu*,[1]

Department of Mechanical Engineering, North Dakota State University, Fargo, ND 58108, USA

HIGHLIGHTS

► Novel unique graphene-beaded carbon nanofibers were synthesized.
► Supercapacitor electrodes based on the new carbon nanostructures were fabricated.
► Microstructures and electrochemical properties of the electrodes were tested.
► Improved electrochemical properties of the novel electrodes were observed.
► Mechanisms responsible for the improved properties were explored.

GRAPHICAL ABSTRACT
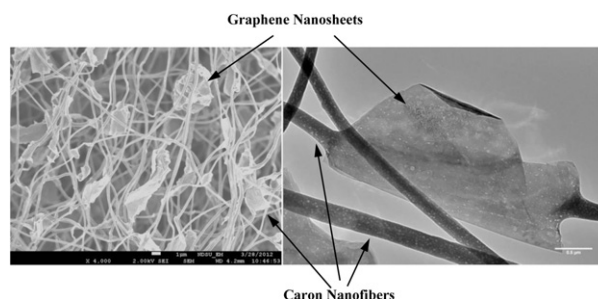
ABSTRACT

This paper studies the synthesis and electrochemical characterization of novel graphene-beaded carbon nanofibers (G/CNFs) as electrode material for use in supercapacitor. The porous G/CNF films were prepared by electrospinning polyacrylonitrile (PAN)/N,N-dimethylformamide (DMF) solution dispersed with oxidized graphene nanosheets, followed by carbonization at 800 °C in a tubular quartz furnace. The morphology and chemical structure of the porous G/CNF films were characterized by means of scanning electron microscopy (SEM), transmission electron microscopy (TEM), and Raman spectroscopy. The electrochemical behavior of the synthesized G/CNF films as supercapacitor electrodes was characterized by means of cyclic voltammetry (CV), galvanotactic charge/discharge, and electrochemical impedance test in a 6 M KOH aqueous electrolyte. Electrochemical measurements revealed that the maximum specific capacitance of the porous G/CNF electrodes reached up to 263.7 F g^{-1} at a discharge current density 100 mA g^{-1}. Furthermore, the supercapacitor exhibited very good cycling stability of energy storage with the retention ratio of 86.9% after 2000 cycles. The high electrochemical performance of the G/CNF electrodes was attributed to the unique nanostructural configuration, high electrical conductivity, and large specific surface area of the graphene nanosheets.

1. Introduction

Supercapacitors [also called ultracapacitors or electrochemical double-layer capacitors (EDLCs)] store and release electrical energy based on the highly reversible electrolyte ions that form an electric double layer at the interface between the porous electrodes and electrolyte [1–3]. Compared to rechargeable batteries, supercapacitors carry much higher specific power density (per unit mass) and energy/power efficiency, faster charge/discharge rate and longer lifetime even in harsh conditions. Supplemental to batteries, supercapacitors have found broad applications in instant switches, portable electronics, backup power supply, regenerative

* Corresponding authors.
    E-mail addresses: zhengping.zhou@ndsu.edu (Z. Zhou), xiangfa.wu@ndsu.edu (X.-F. Wu).
  [1] Tel.: +1 701 231 8836; fax: +1 702 231 8913.

braking system, motor starter, industrial power and energy management, etc. [4–7]. In principle, the specific capacitance of supercapacitor relies highly on the specific surface area of the electrodes and the module voltage [1–3], in which the former is determined by the porosity of the electrode material while the latter is governed by the dielectric properties of the electrolyte. Besides, the energy/power efficiency and lifetime of a supercapacitor also depend upon the internal electrical resistance and electrical contact resistance within the electrodes and between the electrodes and the charge collectors [8]. Due to the low cost and high electrochemical stability, activated carbon has been extensively integrated into commercialized supercapacitors with the capacitance of a unit supercapacitor up to 5000 F [9,10]. Besides, with the recent progress in nanoscience and nanotechnology, carbon nanostructures such as carbon nanotubes (CNTs), carbon nanofibers (CNFs), graphene, etc. have been under intensive investigation as promising candidates of electrode material for use in supercapacitors carrying ultrahigh specific capacitance [11–21].

Among a variety of nanostructured carbon materials, graphene and continuous CNFs have received rapidly growing attention for use in supercapacitors in recent years. Graphene is a two dimensional (2D) carbon material made of monolayered or multilayered graphitic nanosheets [22–24]. Graphene carries exceptional electrical and thermal conductivities, superior mechanical properties, and very large specific surface area (up to 3100 m^2 g^{-1} for individual graphene nanosheets); graphene can also be conveniently fabricated and functionalized [25–31]. To date, exfoliated graphene nanosheets derived from natural graphite have been produced in large scale at low cost, and the process does not seek the aid of extensive chemical oxidation [30]. These graphene nanosheets with the average thickness of 3–5 nm consist typically of a few graphene monolayers and have demonstrated attractive physical and chemical behaviors as a new family of carbon nanomaterials for use in electrochemical energy conversion and storage [32,33]. It has been reported that a number of graphene-based nanomaterials have been integrated into porous electrodes of supercapacitors with high specific capacitance, which are based mainly on the configuration of graphene paper in aqueous electrolyte [34–45]. The resulting specific capacitance depends highly upon the fabrication process of graphene nanosheets. For instance, it is crucial to avoid the aggregation of graphene nanosheets in order to maintain the high specific surface area. Yet, due to the discrete nature of exfoliated graphene or graphitic nanoflakes, the graphene nanosheets stacked loosely in porous electrodes may lead to noticeable electrical contact resistance that may adversely decrease the energy and power efficiencies of the supercapacitors [8]. New techniques and processes are still desired to resolve such a dilemma of achieving the ultrahigh specific surface area while maintaining the electrical connectivity between graphene nanosheets.

On the other hand, electrospinning technique as a low-cost, scalable, top-down nanomanufacturing tool has been commonly considered for producing continuous nanofibers of a broad spectrum of polymers and polymer-derived carbon, metals, metal oxides, ceramics, etc. [46–48]. Electrospinning also provides versatile routes of fabricating low-cost, porous, nanofibrous electrodes for promising use in supercapacitors and rechargeable batteries [49–52]. Among these, continuous CNFs synthesized via carbonization of as-electrospun polymer nanofibers carry excellent electrical and thermal conductivities and high connectivity for transport of electrical and thermal currents, and thus have raised particular interests of materials scientists and engineers worldwide. So far, several types of supercapacitors made of porous electrodes of electrospun CNFs have been successfully demonstrated with high specific capacitance and improved stability [53–59]. Yet, compared to CNTs and graphene, electrospun CNFs

normally carry relatively lower specific surface area, which significantly limits the electrochemical performance of supercapacitors.

In this study, we were to devise a new route for synthesis and characterization of an innovative porous electrode material based on continuous graphene-beaded CNFs (G/CNFs) for use in supercapacitors. The goal was to comprehensively exploit the advantages of electrospun CNFs (e.g., continuity and electrical conductivity) and graphene (e.g., large specific surface area and high electrical conductivity) for the purpose of electrical energy storage. The porous G/CNF films were produced via electrospinning polyacrylonitrile (PAN)/*N,N*-dimethylformamide (DMF) solution dispersed with oxidized graphene nanosheets and consecutive carbonization; the chemical structure and electrochemical properties of the novel G/CNF-based electrodes were characterized and compared with those based on pure electrospun CNFs (without graphene). The rest of the paper is formulated as follows. Section 2 delineates the experimental details to produce and characterize the novel porous G/CNF electrode material. Section 3 describes the experimental measurements and relevant discussions. Consequently, Section 4 addresses the conclusions and prospect of the present study.

2. Experimental

2.1. Materials

Polyacrylonitrile (PAN, $M_w = 150,000$) powder and *N,N*-dimethylformamide (DMF, 99%) were purchased from Sigma–Aldrich Chemical Co. (St. Louis, MO, USA). As-grown, highly graphitic graphene nanosheets were supplied by XG Sciences, Inc. (Lansing, MI, USA). The oxidized graphene nanosheets contained oxygen (<1 wt.%) and had an average thickness of ~6–8 nm and a typical specific surface area of 120–150 m^2 g^{-1}. All the chemicals were used as received without further purification or modification.

2.2. Preparation of porous G/CNF films

Graphene-beaded PAN (G/PAN) nanofibers were produced by electrospinning and used as the precursor for preparing G/CNFs. To electrospin G/PAN nanofibers, a solution consisting of graphene nanosheets and PAN in DMF was prepared as follows. PAN powder was first dissolved in DMF to prepare 15 wt.% PAN solution; well dispersed oxidized graphene nanosheets in DMF by sonication were then added into the PAN/DMF solution to achieve the concentrations of 10 wt.% PAN and 1 wt.% graphene nanosheets in DMF. The solution was kept at a temperature of 80 °C and under continuous stirring on a hotplate for 24 h. During the electrospinning process, the as-prepared solution was then placed into a 10-ml plastic syringe installed with a stainless spinneret, which was connected to a positive high-voltage DC power supply (Gamma High Voltage Research, Inc., Ormond Beach, FL). A laboratory-made rotary aluminum disk with the diameter of 33 cm was electrically grounded and used as the nanofiber collector. A high DC electrical field of 80 kV m^{-1} was generated via applying a positive voltage 20 kV to a 25 cm gap between the spinneret and the grounded nanofiber collector. The flow rate of the electrospinning solution was fixed at 1.0 ml h^{-1} through a digital flow controller. After electrospinning, the gained nonwoven G/PAN nanofiber films were peeled off the aluminum foil on the rotary disk, and then dried in an oven at 100 °C for 6 h prior to the stabilization treatment.

The stabilization and carbonization of the as-prepared G/PAN nanofiber films were performed in a tubular quartz furnace (Atomate, Inc., Santa Barbara, CA). The electrospun G/PAN nanofiber films were first heated up at a rate of 1 °C min^{-1} and maintained at 215 °C for 1 h in air for the purpose of oxidative

stabilization of PAN. The films were then carbonized as the temperature was increased from 215 to 800 °C in Ar atmosphere at a rate of 5 °C min−1 and annealed at 800 °C for 30 min. Thereafter, the quartz furnace was cooled down to 400 °C in Ar and then kept at this temperature by introducing the air for 1 h for activation of the carbonized G/PAN nanofibers.

For the purpose of comparison, pure CNF films as the control samples were also synthesized by using a 10 wt.% PAN/DMF solution under the same process parameters above.

2.3. Characterization

The surface morphology of both the CNF and G/CNF samples was characterized by using a high-resolution field-emission scanning electron microscope (SEM, JEOL JSM-7600F). A transmission electron microscope (TEM, JEOL JEM-2100) was further employed for characterization of the microstructure of the samples (i.e., G/CNFs, CNFs, and G/PAN nanofibers). Before the TEM measurements, the nanofiber samples were first dispersed in acetone and then deposited on a Cu grid. The structural variation of the nanofiber samples was identified by using a laser confocal Raman spectrometer (Nicolet NXR 9650 FT-Raman spectrometer, 632.8 nm).

2.4. Electrochemical measurements

A symmetrical two-electrode cell setup was prepared for the electrochemical characterization of the nanofiber samples because such setup could provide the most accurate electrochemical evaluation [60]. The cell setup was built up with two pieces of 1.0 cm^2 G/CNF films that were attached on a wire fabric; perforated nickel-copper sheets were used as the current collectors; a 6 M KOH aqueous solution was utilized as the working electrolyte in a glass cell. The two current collectors were served to convey the electrical current from one electrode to the other. Cyclic voltammetry (CV) and galvanostatic charge−discharge constant-current test were used to characterize the electrochemical performance of the supercapacitor cells. During the process, the CV and galvanostatic charge−discharge curves were recorded using a battery tester BT2000 (Arbin Instruments, TX, USA) and used for evaluating the capacitive behavior and calculating the specific capacitance of the porous G/CNF electrodes. The CV and galvanostatic charge-discharge measurements of the G/CNF electrodes were performed at the potential range of 0−0.8 V by varying the scan rate from 5 to 100 mV s^{-1}. The electrochemical impedance test was performed on an Electrochemical Multiplexer ECM8 with a frequency in the range of 0.01 Hz−100 kHz.

3. Results and discussions

3.1. Morphology and structure characterization

Digital optical image of the synthesized G/CNF film is shown in Fig. 1(A), from which it can be observed that the carbonized G/PAN nanofibers made from the precursor G/PAN nanofibers still keep the high structural flexibility and in-planar extensibility. With considering the unique topological connectivity and high electrical conductivity of the G/CNF network, the synthesized G/CNF films are suitable for potential use as interconnects and electrodes in stretchable electronic devices. Fig. 1(B) and (C) are the typical SEM micrographs of the CNFs and G/CNFs, respectively. These
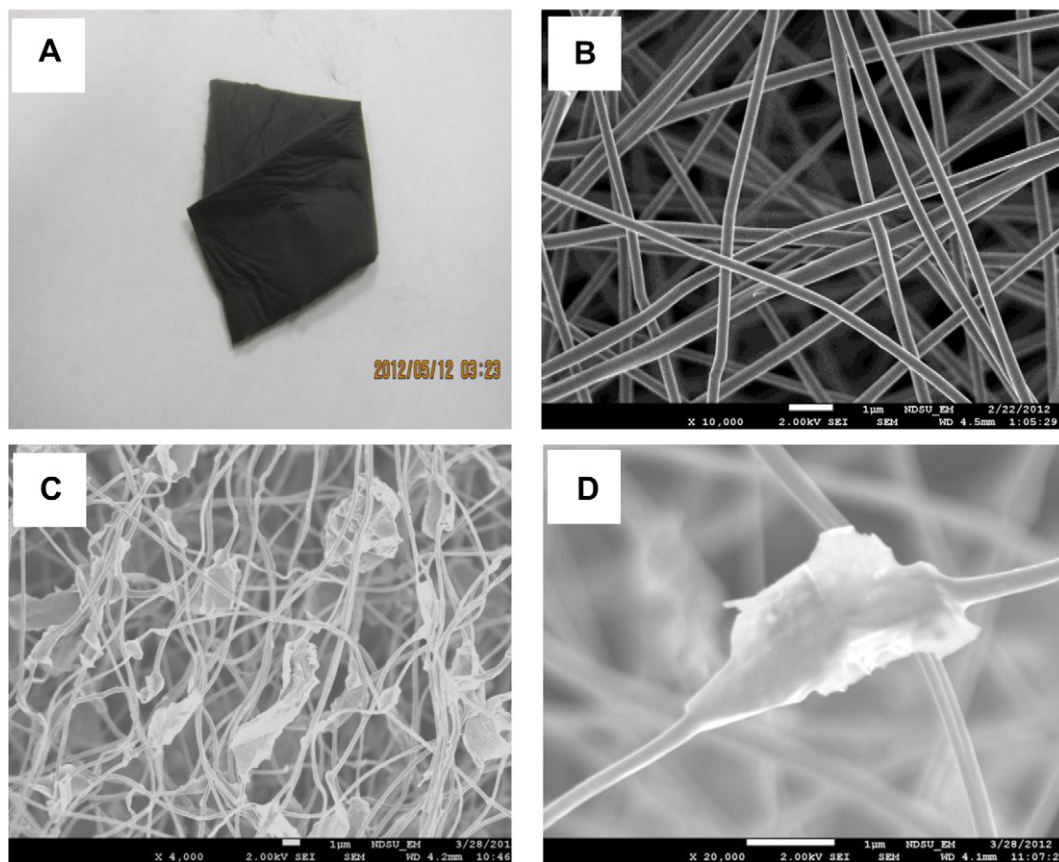

Fig. 1. (A): Digital optical image of a piece of G/CNF film; (B): SEM micrograph of CNFs; and (C) & (D): SEM micrographs of G/CNFs with low and high magnification, respectively.

electrospun CNFs with the diameter ranging from 300 to 400 nm were prepared by carbonization of the precursor as-electrospun PAN nanofibers at 800 °C, and these CNFs carried very smooth surface. In addition, Fig. 1(D) is the high-resolution SEM micrograph of the G/CNFs, from which it can be clearly observed that the graphene nanosheets were closely jointed to the CNF segments after carbonization of the precursor as-electrospun G/PAN nanofibers. These platelet-shaped graphene nanosheets have an average in-planar size of 1—5 microns and an average thickness of 6—8 nm. In general, graphene nanosheets can attain a large surface area and very high electrical conductivity, which may eliminate the need of conductive fillers and result in thinner electrodes.

Fig. 2(A) and (B) are the TEM micrographs of an as-electrospun G/PAN nanofiber segment and the corresponding graphene platelet, respectively. Fig. 2(C) and (D) are the TEM micrographs of the G/CNF nanofiber segments and the corresponding graphene platelet after carbonization, respectively. Obvious difference of the surface morphology between the G/PAN nanofibers and G/CNFs can be identified such that the graphene nanosheets after carbonization exhibited sharper and cleaner edges because the platelets in the as-electrospun G/PAN nanofibers might be covered dusts or solution residues after drying, which were burnt off during the process of carbonization. In addition, as shown in Fig. 2(A) and (C), the graphene nanosheets are firmly connected at two ends with the nanofiber segments before and after carbonization. It is known that the graphene nanosheets were electrospun to form the G/PAN nanofibers, which consequently formed into the G/CNFs after carbonization. It needs to be emphasized that the connection between the graphene nanosheets and the CNF segments could be the strong covalent C—C bonds. Besides, Fig. 2(D) shows a typical linkage between a graphene nanosheet and its substrate amorphous CNF. At the edge of the graphene nanosheet, the graphene plane was detected onto the surface of the nanofiber segment [61]. Such unique morphology would contribute to stabilization of the three-dimensional (3D) structure of the electrodes during the charge-discharge cycling and enhancement of the specific capacitance and cycling life span.

The chemical microstructure of the as-prepared CNFs was characterized by means of Raman spectroscopy in this study. Fig. 3 shows the comparative Raman spectra of CNFs (black, solid) and G/CNFs (red, dotted) in the region of 800—2200 cm^{-1}. The Raman spectra of both the G/CNFs and pure CNFs exhibit two well-known bands of carbon at $\sim$1342 cm^{-1} and $\sim$1567 cm^{-1}, i.e., the "D-band" and "G-band", respectively. The D-band is attributed to the disordered turbostratic structures or defects in the curved graphene nanosheets [62]; the G-band is related to the phonons propagating along the graphitic structures [57]. The intensity ratio of the D peak to the G peak, denoted by $R = I_D/I_G$, represents the amount of ordered graphite crystallites in the CNFs. The R value of G/CNFs is 0.81, much lower than that of CNFs of 1.04. This difference indicates that the G/CNF films have more ordered graphite crystallites than the pure CNF films due to addition of the highly ordered graphitic (graphene) nanosheets ($\sim$20 wt.% in the final G/CNFs). Furthermore, addition of graphene nanosheets into PAN could potentially enhance the transition ratio of disordered carbon into ordered graphite carbon in CNFs during the process of carbonization. The above results on the chemical microstructure clearly demonstrate that the G/CNF films have higher electrical conductivity than the pure CNF films as shown in Fig. 7.

3.2. Electrochemical characterization

To evaluate the electrochemical performance of the pure CNFs and G/CNFs, CV measurements were tested on the CNFs and G/CNFs as the electrodes of supercapacitors in a 6 M KOH aqueous solution, respectively. Fig. 4 shows the typical CV curves of the tested CNF and G/CNF electrodes with a scan rate of 5 mV s^{-1} and a potential window of 0—0.8 V. The CV curve of G/CNF electrodes exhibits a nearly rectangle-shaped profile without obvious redox peaks, which is the characteristic of an ideal double-layer capacitor. In
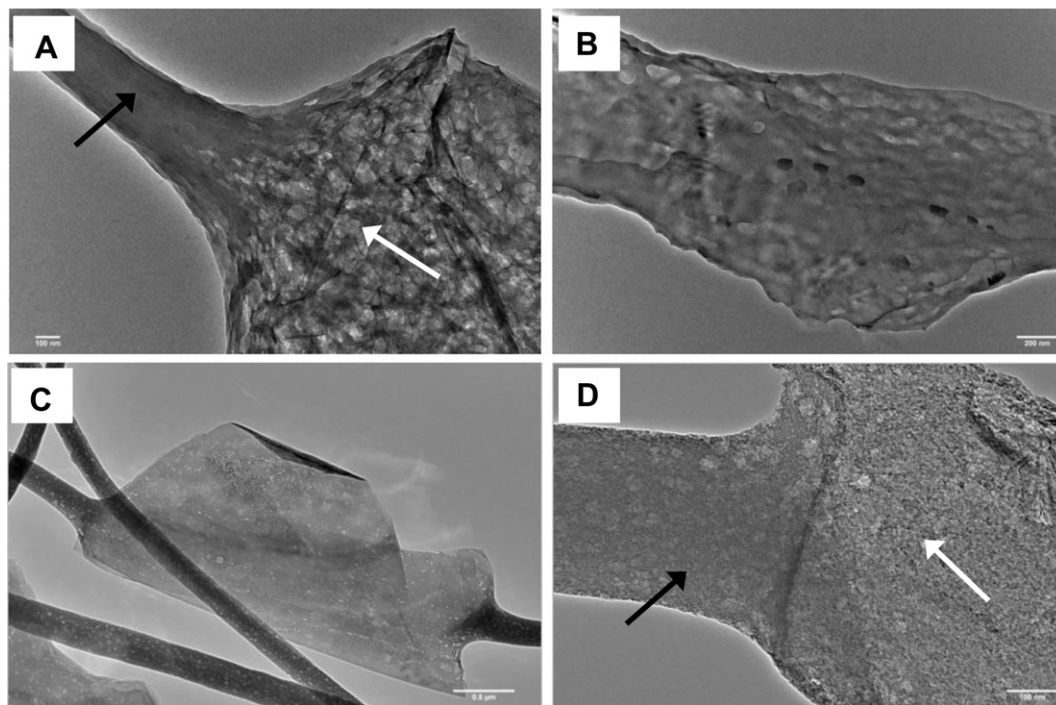

Fig. 2. (A) & (B): TEM micrographs of an electrospun G/PAN nanofiber segment and a graphene nanosheet in G/PAN nanofiber segment before carbonization, respectively; (C) & (D): G/CNF segments at low and high magnifications after carbonization, respectively. The black arrows in micrographs (A) and (D) indicate a precursor G/PAN nanofiber and a G/CNF, respectively; the white arrow marks the graphene nanosheet.
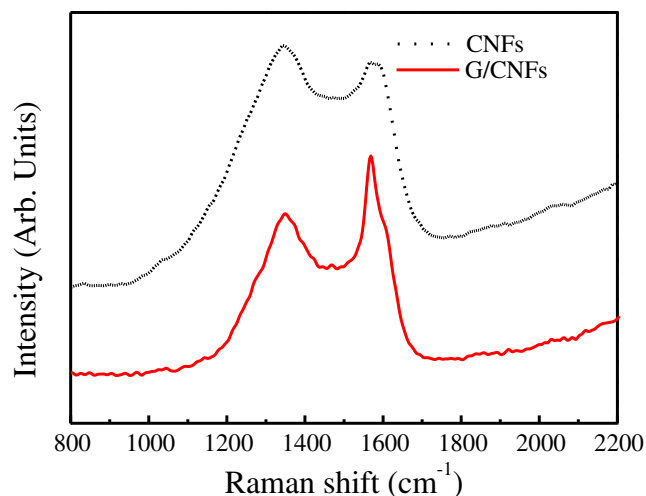
Fig. 3. Raman spectra of CNF (black) and G/CNF (red) samples, respectively. (For interpretation of the references to color in this figure legend, the reader is referred to the web version of this article.)

Fig. 5. Cyclic voltammograms of G/CNF samples at a varying scan rate in the range of 5–100 mV s^{-1}.

contrast, the CV curve of the control CNF electrodes becomes relatively distorted rectangular shape. This difference can be partially attributed to the improved internal electrical conductivity of G/CNF electrodes via graphene nanosheets interlaying. Fig. 5 shows the CV curves of the G/CNF electrodes at different potential scan rates of 5, 10, 30, 50, and 100 mV s^{-1} with the same electrolyte and potential window, respectively. With increasing potential scan rate, the CV profiles still retain a relatively rectangular shape without obvious distortion, even at the scan rate up to 100 mV s^{-1}.

To accurately determine the electrochemical behavior of the novel supercapacitors, the galvanostatic charge-discharge performance of both CNFs and G/CNFs as electrodes was tested at varying current densities. The average specific capacitance (C) of all the porous electrodes in supercapacitor is calculated as

$$C = \frac{I \times \Delta t}{M \times \Delta V},$$ (1)

where I is the constant charge/discharge current (A), Δt is the discharge time (s), ΔV is the potential difference (V) during the

discharge process, and M is the total mass of CNFs of the two electrodes (g). Fig. 6 shows the representative charge/discharge curves of both the pure CNF and G/CNF electrodes at a constant current density of 500 mA g^{-1}. From these curves, the specific capacitance of the G/CNF electrodes is calculated as 226.2 F g^{-1}, twice that of the pure CNF electrodes (114.6 F g^{-1}). It can be observed that a voltage drop existed at the beginning of the discharge curve, i.e., the IR drop that is attributed to the internal resistance of electrodes. Obviously, large internal resistance and contact resistance between the CNFs existed, as evidenced by a noticeable IR drop in the discharge curve in the CNF electrode as shown in Fig. 6. However, the IR drop is significantly lower than that of the CNF electrode. These results indicate that the unique interlaying graphene nanosheets effectively suppressed the internal electrical resistance of the electrodes. To further investigate the impact of internal resistance and interfacial contact resistance on the current collector, electrochemical impedance spectroscopy (EIS) analysis was conducted in the frequency range of 0.01 Hz–100 kHz. The Nyquist plots of the CNF and G/CNF electrodes are shown in Fig. 7. Absence of the semicircle regions in both the plots implies the low faradic resistances of the films and
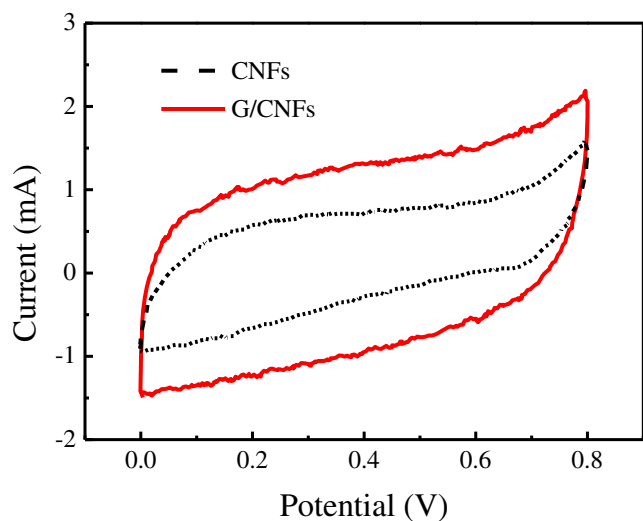

Fig. 4. Cyclic voltammograms of CNF (black) and G/CNF (red) samples at a scan rate of 5 mV s^{-1} in a 6 M KOH solution. (For interpretation of the references to color in this figure legend, the reader is referred to the web version of this article.)
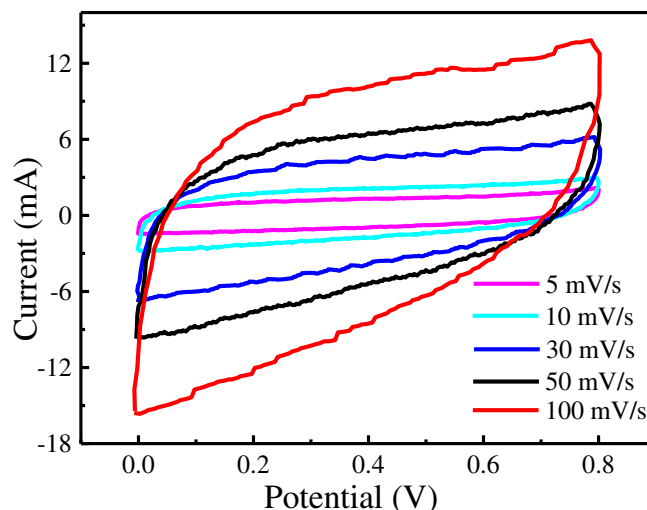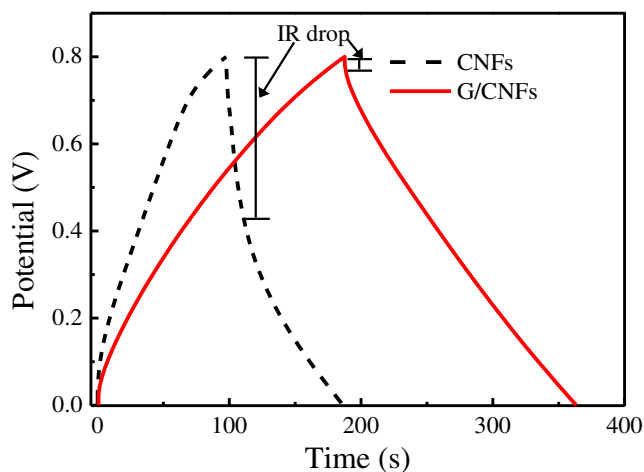

Fig. 6. Galvanostatic charge–discharge curves of CNF (black) and G/CNF (red) samples at a constant current density of 500 mA g^{-1}. (For interpretation of the references to color in this figure legend, the reader is referred to the web version of this article.)
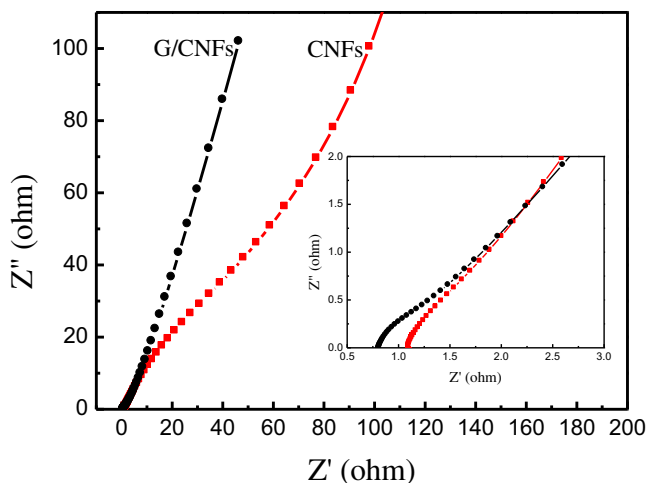
Fig. 7. Nyquist plots for the G/CNF (black) and CNF (red) electrodes in the frequency range of 0.01 Hz–100 kHz. Z' is the real part of the complex impedance. Z'' is the imaginary part of the complex impedance. The inserted plot shows the impedance spectra at the high frequency region. (For interpretation of the references to color in this figure legend, the reader is referred to the web version of this article.)

good electrical conductivity between the nanofibers and current collectors [39]. The inserted sub-plot in Fig. 7 shows of the impedance spectra at the high frequency region. It has been shown that the internal resistances of the CNF and G/CNF electrodes are 1.1 Ω and 0.8 Ω, respectively. These results imply that the graphene nanosheets suppressed the electrode resistance, corresponding to a smaller IR drop as observed in Fig. 6. The values of specific capacitance of the G/CNF electrodes as a function with respect to the discharge current density from 100 mA g^{-1} to 5 A g^{-1} are plotted in Fig. 8. In general, the specific capacitance decreases slightly with increasing discharge current density. The maximum specific capacitance of G/CNF electrodes reached the value of 263.7 F g^{-1} at a discharge current density of 100 mA g^{-1}. It is noteworthy that the specific capacitance of the G/CNF electrodes still remained a high value of 131.25 F g^{-1} even at a high discharge current density up to 2.5 A g^{-1}. Also, the measured highest specific capacitance of G/CNF electrodes (263.7 F g^{-1}) is higher than the estimated specific capacitance ($\sim$175 F g^{-1}) based on the mass ratio ($\sim$50%) of graphene in G/CNFs and the specific capacitances of CNFs ($\sim$150 F g^{-1}) and graphene nanosheets ($\sim$200 F g^{-1}) reported in the literature. It needs to be mentioned that the capacitance of graphene nanosheets reported in the literature was measured using randomly stacked graphene electrodes, in which the graphene nanosheets could be commonly stacked each other and thus charges could not be fully stored on all the surfaces of the individual nanosheets. Thus, the specific capacitance of stacked graphene nanosheets would be much smaller than that of nearly free-standing individual graphene nanosheets, like the ones in G/CNFs.

Furthermore, electrochemical stability is one of the crucial factors to supercapacitors for any practical use [58]. The cycling life test of the CNF and G/CNF based supercapacitors had been performed in a 6 M KOH aqueous solution over 2000 cycles. Constant current cycling was performed at a current rate of 2.5 A g^{-1} between 0 and 0.8 V. Fig. 9 shows the specific capacitance retention ratio of the CNF and G/CNF electrodes as a function of the cycle number. The supercapacitor retention ratios of CNF and G/CNF electrodes were 75.6% and 86.9% after 2000 cycles, respectively. This implies that incorporation of graphene nanosheets into the carbonized PAN nanofibers had a significant influence on the cyclic durability of the supercapacitor during the cycling charge/discharge process. Within the G/CNFs, graphene nanosheets acted
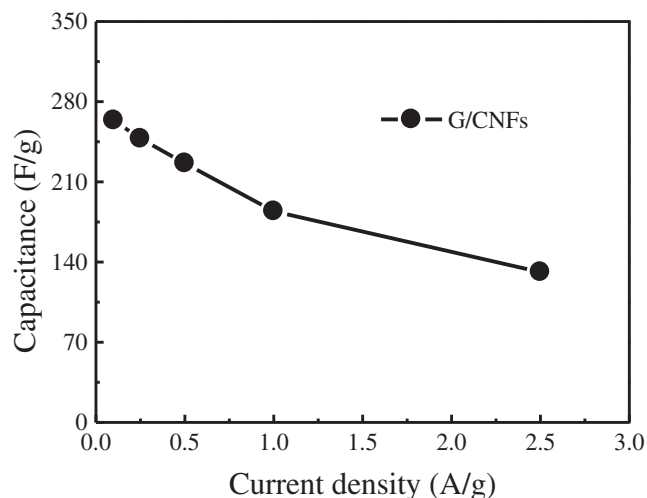

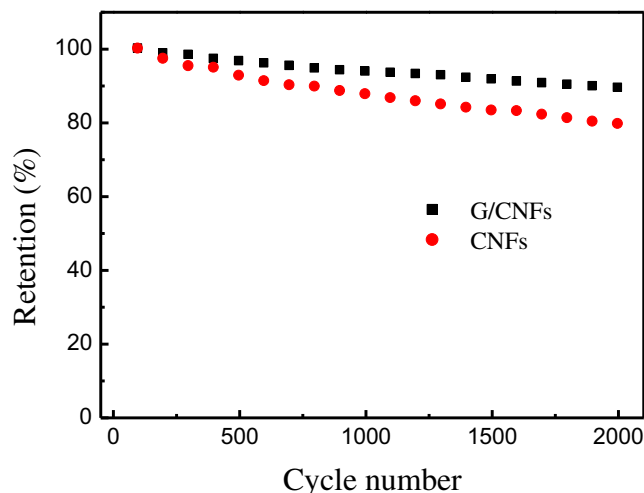**Fig. 8.** Variation of the specific capacitance of G/CNFs with the current density.

Fig. 9. Cycling performance of the G/CNF (black) and CNF (red) electrodes at a constant current density of 2.5 A g^{-1}. (For interpretation of the references to color in this figure legend, the reader is referred to the web version of this article.)

as interconnectors for improving the internal electrical conductivity and enhancing the specific surface area of the electrodes for charge storage. Meanwhile, the substrate CNFs also acted as frameworks to bridge the graphene nanosheets and prevent the nanosheets from severe swelling and shrinking during the cycling process [34]. Also, the retention ratio (86.9%) of G/CNF electrodes after 2000 cycles is lower than that of activated carbon ($\sim$95%) after the similar cycles though the G/CNF electrodes still carry the specific capacitance higher than that of activated carbon. The possible reconfiguration of the nearly free-standing graphene nanosheets in G/CNF electrode at high current density (2.5 A G^{-1}) could be responsible the fast decrease of the retention ratio of G/CNF electrodes with the cycling number in the present study. Thus, further investigation is still desired for exploring the potential mechanisms of such a fast retention decrease and finding new routes to optimize the material design and selection for enhanced capacitive performance of the novel G/CNF electrodes in this study.

4. Conclusions

Successful synthesis and structural/electrochemical characterization of a novel porous G/CNF-based electrode material for use in

high-performance supercapacitors has been demonstrated. During the process, the porous G/CNFs have been successfully synthesized by electrospinning the solution of PAN/DMF dispersed with oxidized graphene nanosheets, followed by carbonization in a tubular quartz furnace. One of the major benefits of the study is that the graphene nanosheets with excellent 2D nanostructures and electrical properties can be embedded along with CNFs to achieve attractive chemical structure and superior surface morphology. The excellent connectivity of the graphene nanosheets embedded in carbonized PAN nanofibers significantly improved the specific surface area and electrical conductivity of the resulting G/CNFs. These free-standing, flexible films can be directly used as electrodes in supercapacitors without the aid of polymer binder. The novel porous G/CNF films exhibit superior electrochemical properties for potential use in high-capacitance EDLCs. New technical routes are still needed to enhance the capacitance retention ratio of such novel G/CNF-based supercapacitors for promising use in electrical energy conversion and storage.

Acknowledgment

References

[1] M. Winter, R.J. Brodd, Chem. Rev. 104 (2004) 4245−4269.
[2] B.E. Conway, J. Electrochem. Soc. 138 (1991) 1539−1547.
[3] R. Kötz, M. Carlen, Electrochim. Acta 45 (2000) 2483−2498.
[4] J.R. Miller, P. Simon, Science 321 (2008) 651−652.
[5] P. Harrop, H. Zervos, Batteries, Supercapacitors, Alternative Storage for Portable Devices 2009−2019, IDTechEx, Cambridge, MA, USA, 2009.
[6] J.R. Miller, A.F. Burke, Electrochem. Soc. Interface 17 (2008) 53−57.
[7] B. Andrew, J. Power Sourc. 91 (2000) 37−50.
[8] X.F. Wu, Z.P. Zhou, W.M. Zhou, Appl. Phys. Lett. 100 (2012) 193115−193118.
[9] E. Frackowiak, F. Béguin, Carbon 39 (2001) 937−950.
[10] A.G. Pandolfo, A.F. Hollendamp, J. Power Sourc. 157 (2006) 11−27.
[11] J. Chmiola, G. Yushin, Y. Gogotsi, C. Portet, P. Simon, P.L. Taberna, Science 313 (2006) 1760−1763.
[12] V.V.N. Obreja, Physica E 40 (2008) 2596−2605.
[13] L.L. Zhang, X.S. Zhao, Chem. Soc. Rev. 38 (2009) 2520−2531.
[14] M. Inagaki, H. Konno, O. Tanaike, J. Power Sourc. 195 (2010) 7880−7903.
[15] A.S. Aricò, P. Bruce, B. Scrosati, J.M. Tarascon, W.V. Schalkwijk, Nat. Mater. 4 (2005) 366−377.
[16] P. Simon, Y. Gogotsi, Nat. Mater. 7 (2008) 845−854.
[17] M.S. Whittingham, MRS Bull. 33 (2008) 411−420.
[18] D.S. Su, R. Schlögl, ChemSusChem 3 (2010) 136−168.
[19] C. Liu, F. Li, L.P. Ma, H.M. Cheng, Adv. Mater. 22 (2010) E28−E62.
[20] X. Zhao, B.M. Sánchez, P.J. Dobson, P.S. Grant, Nanoscale 3 (2011) 839−855.
[21] P. Balaya, Energy Envir. Sci. 1 (2008) 645−654.
[22] A.K. Geim, Science 324 (2009) 1530−1534.
[23] M.I. Katsnelson, Mater. Today 10 (2007) 20−27.
[24] K.S. Novoselov, Rev. Mod. Phys. 83 (2011) 837−849.
[25] A.A. Balandin, S. Ghosh, W.Z. Bao, I. Calizo, D. Teweldebrhan, F. Miao, C.N. Lau, Nano Lett. 8 (2008) 902−907.
[26] A.H.C. Neto, F. Guinea, N.M.R. Peres, K.S. Novoselov, A.K. Geim, Rev. Mod. Phys. 81 (2009) 109−162.
[27] C. Lee, X.D. Wei, J.W. Kysar, J. Hone, Science 321 (2008) 385−388.
[28] D.R. Dreyer, S. Park, C.W. Bielawski, R.S. Ruoff, Chem. Soc. Rev. 39 (2010) 228−240.
[29] K.P. Loh, Q.L. Bao, P.K. Ang, J.K. Yang, J. Mater. Chem. 20 (2010) 2277−2289.
[30] L.T. Drzal, H. Fukushima. U.S. Patent 20040127621 2004.
[31] W.B. Wan, Z.B. Zhao, Y.R. Fan, H. Hu, Q. Zhou, J.S. Qiu, Prog. Chem. 23 (2011) 1883−1891.
[32] D.A.C. Brownson, D.K. Kampouris, C.E. Banks, J. Power Sources 196 (2011) 4873−4885.
[33] S. Biswas, L.T. Drzal, ACS Appl. Mater. Interfaces 2 (2010) 2293−2300.
[34] M.D. Stoller, S.J. Park, Y.W. Zhu, J. An, R.S. Ruoff, Nano Lett. 8 (2008) 3498−3502.
[35] W. Lv, D.M. Tang, Y.B. He, C.H. You, Z.Q. Shi, X.C. Chen, C.M. Chen, P.X. Hou, C. Liu, Q.H. Yang, ASC Nano 3 (2009) 3730−3736.
[36] S. Chen, J.W. Zhu, X.D. Wu, Q.F. Han, X. Wang, ASC Nano 4 (2010) 2822−2830.
[37] C.G. Liu, Z.N. Yu, D. Neff, A. Zhamu, B.Z. Jang, Nano Lett. 10 (2010) 4863−4868.
[38] J.R. Miller, R.A. Outlaw, B.C. Holloway, Science 329 (2010) 1637−1639.
[39] Q. Wu, Y.X. Xu, Z.Y. Yao, A.R. Liu, G.Q. Shi, ACS Nano 4 (2010) 1963−1970.
[40] J. Yang, Z.J. Fan, T. Wei, W.Z. Qian, M.L. Zhang, F. Wei, Carbon 48 (2010) 3825−3833.
[41] D.S. Yu, L.M. Dai, J. Phys. Chem. Lett. 1 (2010) 467−470.
[42] K. Zhang, L.L. Zhang, X.S. Zhao, J.S. Wu, Chem. Mater. 22 (2010) 1392−1401.
[43] Y.W. Zhu, S. Murali, M.D. Stoller, K.J. Ganesh, W.W. Cai, P.J. Ferreira, A. Pirkle, R.M. Wallace, K.A. Cychosz, M. Thommes, D. Su, E.A. Stach, R.S. Ruoff, Science 332 (2011) 1537−1541.
[44] M.F. El-Kady, V. Strong, S. Dubin, K.B. Kaner, Science 335 (2012) 1326−1330.
[45] J. Yan, J.P. Liu, Z.J. Fan, T. Wei, L.J. Zhang, Carbon 50 (2012) 2179−2188.
[46] D.H. Reneker, I. Chun, Nanotechnology 7 (1996) 216−223.
[47] D.H. Reneker, A.L. Yarin, E. Zussman, H. Xu, Adv. Appl. Mech. 41 (2006) 43−195.
[48] D.H. Reneker, A.L. Yarin, Polymer 49 (2008) 2387−2425.
[49] M.J. Laudenslager, R.H. Scheffler, W.M. Sigmund, Pure Appl. Chem. 82 (2010) 2137−2156.
[50] J.J. Miao, M. Miyauchi, T.J. Simmons, J.S. Dordick, R.J. Linhardt, J. Nanosci. Nanotech 10 (2010) 5507−5519.
[51] Z.X. Dong, S.J. Kennedy, Y.Q. Wu, J. Power Sources 196 (2011) 4886−4904.
[52] X.W. Zhang, L.W. Ji, O. Toprakci, Y.Z. Liang, M. Alcoutlabi, Polym. Rev. 51 (2011) 239−264.
[53] C. Kim, K.S. Yang, Appl. Phys. Lett. 83 (2003) 1216−1218.
[54] C. Kim, Y.O. Choi, W.J. Lee, K.S. Yang, Electrochim. Acta 50 (2004) 883−887.
[55] Q.H. Guo, X.P. Zhou, X.Y. Li, S.L. Chen, A. Seema, A. Greiner, H.Q. Hou, J. Mater. Chem. 19 (2008) 2810−2816.
[56] E.J. Ra, E. Raymundo-Piñero, Y.H. Lee, F. Béguin, Carbon 47 (2009) 2984−2992.
[57] V. Barranco, M.A. Lillo-Rodenas, A. Linares-Solano, A. Oya, F. Pico, J. Ibanez, F. Agullo-Rueda, J.M. Amarilla, J.M. Rojo, J. Phys. Chem. C 114 (2010) 10302−10307.
[58] Y. Hou, Y.W. Cheng, T. Hobson, J. Liu, Nano Lett. 10 (2010) 2727−2733.
[59] Z.P. Zhou, X.F. Wu, H. Fong, Appl. Phys. Lett. 100 (2012) 023115−023118.
[60] V. Khomenko, E. Frackowiak, F. Béguin, Electrochim. Acta 50 (2005) 2499−2506.
[61] C.L. Lai, Q.H. Guo, X.F. Wu, D.H. Reneker, H.Q. Hou, Nanotechnology 19 (2008) 195303−195309.
[62] Z.P. Zhou, K.M. Liu, C.L. Lai, L.F. Zhang, J.H. Li, H.Q. Hou, D.H. Reneker, H. Fong, Polymer 51 (2010) 2360−2367.